RESEARCH ARTICLE
SPACE PHYSICS: IONOSPHERIC PHYSICS

Earth and Planetary Physics
5: 378–386, 2021
doi: 10.26464/epp2021039

On the solar activity dependence of midnight equatorial plasma bubbles during June solstice periods

K. K. Ajith[1*], S. Tulasi Ram[2], GuoZhu Li[1,3,4], M. Yamamoto[5], K. Hozumi[6], C. Y. Yatini[7], and P. Supnithi[8]

[1]Key Laboratory of Earth and Planetary Physics, Institute of Geology and Geophysics, Chinese Academy of Sciences, Beijing 100029, China;

[2]Indian Institute of Geomagnetism, Mumbai, India;

[3]Beijing National Observatory of Space Environment, Institute of Geology and Geophysics, Chinese Academy of Sciences, Beijing 100029, China;

[4]College of Earth and Planetary Sciences, University of Chinese Academy of Sciences, Beijing 100049, China;

[5]Research Institute for Sustainable Humanosphere, Kyoto University, Uji, Japan;

[6]National Institute of Information and Communications Technology, Tokyo, Japan;

[7]Space Science Center, Indonesian National Institute of Aeronautics and Space, Indonesia;

[8]School of Engineering, King Mongkut's Institute of Technology Ladkrabang, Chalongkrung Rd, Ladkrabang, 10520 Bangkok, Thailand

Key Points:

- The solar activity dependence on the occurrence of midnight EPBs were investigated during the ascending phase of solar cycle 24.
- The enhanced flux tube integrated growth rate of RT instability is observed during the low solar active June solstice.
- The elevated F layer and possible seeding by MSTIDs sets the conditions favorable during the low solar active summertime midnight hours.

Citation: Ajith, K. K., Ram, S. T., Li, G. Z., Yamamoto, M., Hozumi, K., Yatimi, C. Y., and Supnithi, P. (2021). On the solar activity dependence of midnight equatorial plasma bubbles during June solstice periods. *Earth Planet. Phys.*, *5*(5), 378–386. http://doi.org/10.26464/epp2021039

Abstract: The occurrence of midnight Equatorial Plasma Bubbles (EPBs) during the June solstice period of the ascending phase of solar cycle 24, from 2010 to 2014, was studied using data from the 47 MHz Equatorial Atmosphere Radar (EAR) at Kototabang, Indonesia. The analysis shows that the occurrence of midnight hour EPBs was at its maximum during the low solar activity year 2010 and monotonically decreased thereafter with increasing solar activity. Details of the dependence of midnight hour EPB occurrence on solar activity were investigated using SAMI2 model simulation with a realistic input of $\boldsymbol{E}\times\boldsymbol{B}$ drift velocity data obtained from the CINDI-IVM onboard the C/NOFS satellite. Results obtained from term-by-term analysis of the flux tube integrated linear growth rate of RT instability indicate that the formation of a high flux tube electron content height gradient (steep vertical gradient) region at higher altitudes, due to the elevated F layer, is the key factor enhancing the growth rate of RT instability during low solar activity June solstices. Other factors are discussed in light of the relatively weak westward zonal electric field in the presence of the equatorward neutral wind and north-to-south transequatorial wind around the midnight hours of low solar activity June solstices. Also discussed are the initial seeding of RT instability by MSTIDs and how the threshold height required for EPB development varies with solar activity.

Keywords: equatorial plasma bubbles; equatorial ionosphere; ionospheric instabilities and irregularities

1. Introduction

The development of Equatorial Plasma Bubble (EPB) irregularities during the night-time equatorial ionosphere causes severe outages in trans-ionospheric radio communications and satellite-based navigation systems. These plasma irregularities are developed at the bottom side F layer through the Rayleigh–Taylor (RT) instability mechanism (Haerendel, 1973; Sultan, 1996) and grow nonlinearly to the topside ionosphere via their interior polarization electric field. The pre-reversal enhancement (PRE) of the zonal electric field and steep density gradient due to bottom side recombination create the conditions that favor the development of EPBs during the post-sunset hours. It has been observed that most of the EPBs are generated just after the sunset and traverse eastward with velocities ranging from 50–200 m/s, and then cease around midnight (Arons et al., 1980; Yokoyama et al., 2004).

However, other studies have reported that EPBs can develop even around and after the midnight period of June solstices (Patra et al., 2009; Ajith et al., 2015). The occurrence characteristics and morphological features of these midnight EPBs have been studied using various observational techniques, which include Ionosonde, VHF scintillation, VHF radar, and topside in situ observations from low-Earth orbiting satellites (Krishna Murthy et al.,

Correspondence to: K. K. Ajith, ajithkk2007@gmail.com
Received 30 MAR 2021; Accepted 17 JUN 2021.
Accepted article online 14 JUL 2021.

1979; Subbarao and Krishna Murthy, 1994; Patra et al., 2009; Li et al., 2011; Yokoyama et al., 2011). Otsuka et al. (2009) reported that most post-midnight EPBs do not show any clear zonal propagation, some of them (35%) exhibiting westward propagation. Using fan sector backscatter observations from Equatorial Atmosphere Radar (EAR) over Kototabang, Indonesia, Ajith et al. (2015) confirmed that most of these midnight hour June solstice EPBs develop freshly in the midnight hours. Further, Dao et al. (2016) and Tulasi Ram et al. (2017) estimated the vertical rise velocity of both post-sunset and post-midnight EPBs and showed that the rise velocity of post-midnight EPBs is much lower than the velocity of post-sunset EPBs. Later, using SAMI2 model simulation, Ajith et al. (2016) confirmed the role of RT instability in the development of EPBs over the Indonesian sector in the midnight hours of June solstices. From all of these studies, it is clear that the characteristic features of midnight hour EPBs are quite different from those of post-sunset EPBs.

So far, many studies have been conducted to understand the solar activity dependence of EPBs. The occurrence probability of post-sunset EPBs has been found to be higher during high solar activity periods (Fejer et al., 1979; Jayachandran et al., 1993; Tulasi Ram et al., 2006). However, the effect of solar activity variations on midnight EPBs shows a different occurrence pattern; it is clear that the occurrence of midnight EPBs is maximized during low solar activity June solstice periods (Otsuka et al., 2009; Heelis et al., 2010; Yizengaw et al., 2013). Thus, it is important to understand the background ionospheric conditions conducive for the development of these EPBs around and after the midnight hours during low solar activity periods. In the present study, we have used data from the Equatorial Atmosphere Radar (EAR), collected over the Indonesian sector during the June solstice periods of the ascending phase of solar cycle 24 (2010–2014), to investigate how the development of midnight EPBs depends on solar activity. Further, we have used multi-instrumental and modelling studies to examine the solar activity effect on the background ionospheric conditions such as $\boldsymbol{E}$ x $\boldsymbol{B}$ drift, electron density, meridional neutral wind, and base height variation (h'F) of the F layer during this period.

2. Data and Observations

The 47 MHz Equatorial Atmosphere Radar (EAR) in Kototabang, Indonesia (0.20°S, 100.32°E, 10.36°S dip latitude) is operated with a peak power of 100 kW and average power of 5 kW. The EAR is regularly operated at 16 beams of F region mode to study the field-aligned irregularities (FAI) at ~3 m scale during night hours (18:00–06:00 LT). The active phased array antenna systems enable EAR to steer the beams on a pulse-to-pulse basis in order to obtain two-dimensional snapshots of backscatter echoes (Fukao et al., 2003). The data from the frequency-modulated continuous wave (FMCW) ionosonde operated at Chumphon (10.7°N geographic latitude, 99.4°E geographic longitude, and 3.3°N geomagnetic latitude) and Kototabang under the South East Asia Low-latitude Ionospheric Network (SEALION) have been used to obtain the base height (h'F) variation of F layer. The Ion Velocity Meter (IVM) on board the Communication/Navigation Outage Forecasting System (C/NOFS) satellite (de La Beaujardière and The C/NOFS Science Definition Team, 2004) were used to estimate the vertical $\boldsymbol{E}$ x $\boldsymbol{B}$ drift velocities during 2010, 2011, 2012, and 2014 over 80°–120° longitude. In 2013, during June–October, the C/NOFS satellite was place in safe mode; hence there was no $\boldsymbol{E}$ x $\boldsymbol{B}$ drift data coverage in 2013. The $\boldsymbol{E}$ x $\boldsymbol{B}$ drift velocity data derived from the C/NOFS-IVM were fed to drive the SAMI2 model (SAMI2 is Another Model of the Ionosphere) to reconstruct the background vertical electron density distributions and compute the flux tube integrated growth rate of RT instability. SAMI2 is a low latitude ionospheric model developed by the Naval Research Laboratory (NRL) to describe the plasma along the Earth's dipole magnetic field (Huba et al., 2000). The model includes input parameters such as $\boldsymbol{E}$ x $\boldsymbol{B}$ drift and $F_{10.7}$ index to reproduce more effectively the solar activity variation in the electron density distribution.

In order to understand how the development of summer time midnight EPBs depends on background ionospheric conditions and solar activity, we have selected only the EPBs that developed freshly over EAR location during the midnight hours (22:00–02:00 LT) of June solstice (May, June, July and August). Limiting this study to freshly developed EPBs excludes EPBs that may have drifted into the observed location after developing elsewhere under unknown background atmospheric and ionospheric conditions. Figure 1 shows an example of a midnight EPB that evolved freshly within the Field of View (FoV) of EAR. It can be seen that no backscatter echoes were observed at 00:52 LT in Figure 1. At 00:54 LT a faint backscatter echo is starting to develop at approximately 250 km altitude. As time progresses, the EPB grows in size and echo intensity. In the present study, we have selected only EPBs of this sort (ones that originated and were observed to grow within the FoV of EAR) during 2010–2014. The annual occurrence statistics of such freshly developed midnight EPBs during June solstice for the years 2010–2014 are given in Table 1.

Table 1. The annual occurrence statistics of freshly developed midnight EPBs during June solstice for the years 2010–2014.

June solstice			
Year	Days having observation	No. of fresh midnight EPBs	Percentage occurrence (%)
2010	56	27	48.2
2011	97	34	35
2012	110	13	11.8
2013	96	6	6.2
2014	92	5	5.4

3. Results

In this study, the summer time midnight EPBs observed from EAR during the geomagnetically quiet (Kp < 3) periods of 2010–2014 were considered. Using frame-by-frame analysis of two dimensional fan sector maps of EAR data we have obtained the occurrence pattern of freshly evolved midnight EPBs during this period. The percentage occurrence of freshly evolved midnight EPBs during the June solstice of 2010–2014 is presented in Figure 2. The red curve in Figure 2 shows the yearly averaged $F_{10.7}$ index. During this period, the yearly mean $F_{10.7}$ index varies from a minim-

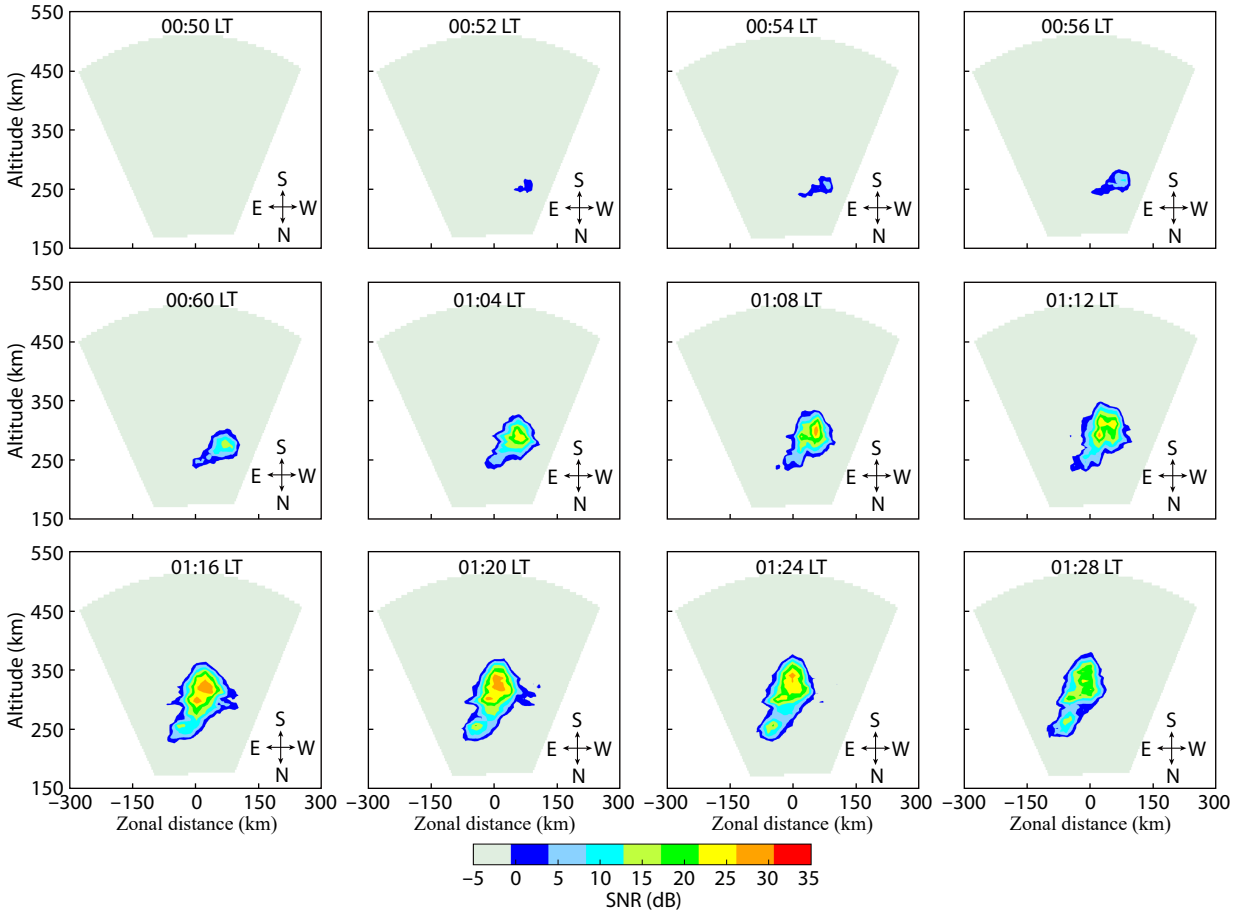

Figure 1. An example showing the onset and successive development of fresh midnight EPB obtained from the 16 beams of EAR on 22 July 2011.

um of 80 sfu (solar flux unit = 10^{-22} $Wm^{-2}Hz^{-1}$) during 2010 to a maximum of 145.9 sfu during 2014. From the figure it can be observed that the highest percentage (48.2%) of summertime midnight EPBs occurred during the low solar activity year 2010. The percentage occurrence decreased monotonically with the increasing solar activity in the following years, reaching its minimum (5.4%) during 2014, demonstrating anti-correlation with solar activity.

To understand the effect of solar activity on the background ionospheric conditions during these summertime midnight periods, we have examined the variation of different ionospheric parameters during 2010–2014. Previous studies have reported that the F layer is elevated to higher altitudes prior to the development of midnight hour June soltice EPBs (Nishioka et al., 2012). Hence, bottom-side F layer virtual height variation (*h*'F) data were estimated using the ionosonde located in the equatorial station Chumphon and low-latitude station Kototabang. Figure 3 shows the variation of *h*'F over Chumphon (solid lines) and Kototabang (dashed lines) during the June solstice periods of 2010–2014. Different colours in Figure 3 indicate the *h*'F observations for different years. The Chumphon ionosonde data during 2011–2012 and Kototabang ionosonde data for the years 2013–2014 were not available due to operational difficulties. From Figure 3, it can be observed that the *h*'F at Chumphon exhibits a clear post sunset

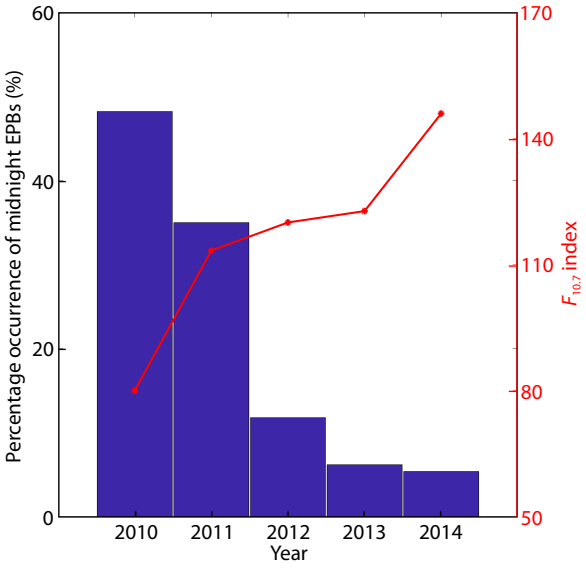

Figure 2. Histogram showing the occurrence of freshly evolved summertime (May, June, July, August) midnight EPBs over Kototabang during the ascending phase of solar cycle 24 (2010–2014). The red curve shows the yearly averaged $F_{10.7}$ index during 2010–2014.

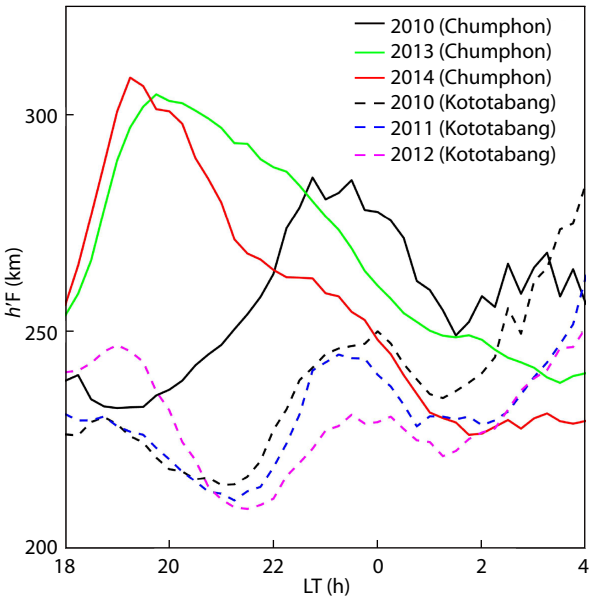

Figure 3. The night time mean *h*′F variation over equatorial station Chumphon and low latitude station Kototabang during June solstice of 2010–2014 (The Chumphon and Kototabang ionosonde data for the years 2011–2012 and 2013–2014 respectively were not available due to operational difficulties).

height rise (PSSR) due to the pre-reversal enhancement (PRE) during the high solar activity years 2013 (with maximum height of 305 km at 19:45 LT — green solid curve) and 2014 (with maximum height of 309 km at 19:15 LT — red solid curve). After the post-sunset maximum, *h*′F decreases rapidly with local time during these years. However, the *h*′F over Chumphon during the low solar activity year 2010 (black solid line) does not exhibit any PSSR. Whereas, *h*′F shows a clear increase after the post-sunset hours and reaches maximum altitude of 285 km around the midnight hours. Similar increase in *h*′F around the midnight hours can be observed over Kototabang during 2010–2012 (dotted lines). It can be noticed that the relatively moderate solar activity year 2012 exhibits a significantly smaller midnight F layer uplift in comparison to the low solar activity years 2010 and 2011. The simultaneous *h*′F observations over Chumphon (black solid curve) and Kototabang (black dotted curve) during 2010 show that the F layer is elevated to a much higher altitude at the equatorial station Chumphon as compared to the low latitude station Kototabang. Further, the F layer uplift during the midnight period over Kototabang shows a clear decrease with increasing solar activity. A similar decrease in the F layer altitude with increasing solar activity can be expected over the equatorial station Chumphon during 2011 and 2012. In summary, the F layer is uplifted to higher altitudes during the midnight hours of low solar activity years and the uplift is reduced with increasing solar activity. We conclude that this uplift of the F layer to higher altitudes during low solar activity June solstices is an important factor behind the onset of midnight EPBs during this period.

With a view to further understand the effect of solar activity on the background zonal electric field during the midnight hours we have estimated the background $\boldsymbol{E} \times \boldsymbol{B}$ drift velocity using the

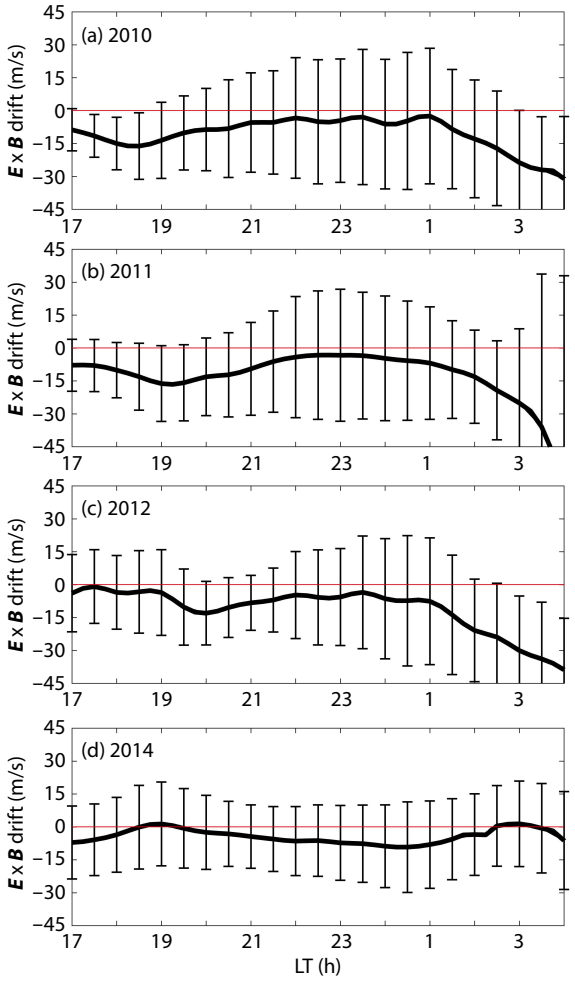

Figure 4. The mean $\boldsymbol{E} \times \boldsymbol{B}$ drift as a function of local time for June solstice obtained from CINDI-IVM onboard the C/NOFS satellite for the years (a) 2010, (b) 2011, (c) 2012, and (d) 2014 respectively.

CINDI-IVM on board the C/NOFS satellite. Following the method used in Stoneback et al., (2011), the $\boldsymbol{E} \times \boldsymbol{B}$ drift velocities in the present analysis are taken for the entire latitude range of C/NOFS data over 80°–120° longitude for the Indonesian region. To avoid geomagnetically disturbed periods, the data are selected only for days with $Kp < 3$. To ensure sufficient signal to the drift meter, the satellite altitude is limited to 400–550 km and the lower limit for O^+ concentration is set at 3×10^3 cm^{-3}. Finally, the mean $\boldsymbol{E} \times \boldsymbol{B}$ drift velocities are calculated by averaging them for each 30-minute interval of local time, from 17:00 to 04:00 LT, for the June Solstice periods of years 2010, 2011, 2012, and 2014. The local time variations of these mean $\boldsymbol{E} \times \boldsymbol{B}$ drift velocities are presented in Figure 4. The thick black curve in Figure 4 indicates the mean drift velocity; the standard deviation is represented by error bars. From Figure 4 it is clear that the $\boldsymbol{E} \times \boldsymbol{B}$ drift is largely negative (downward) during the post sunset hours of 2010, 2011, and 2012. It is interesting to observe that $\boldsymbol{E} \times \boldsymbol{B}$ drift starts increasing after the sunset hours and exhibits a broad peak between 22:00 and 02:00 LT with maximum values of –1.7 m/s, –3.26 m/s, and –3.96 m/s for the years 2010, 2011, and 2012 respectively. On the other hand, in 2014 the $\boldsymbol{E} \times \boldsymbol{B}$ drift is slightly positive (upward) during the post-sunset hours and decreases with local time (without any mid-

night enhancement). Similar to the *h*'F observations (Figure 3), the $\boldsymbol{E}\times\boldsymbol{B}$ drift values during the post-sunset hours are increasing with increasing solar activity; around the midnight hours they decrease with increasing solar activity. In a nutshell, the presence of the weak westward electric field during the midnight period of low solar activity years might be the one important factor that helps the F layer to remain at higher altitude due to the absence of large downward $\boldsymbol{E}\times\boldsymbol{B}$ drift.

In the present study, our aim is to examine the effect of solar activity on the background atmospheric and ionospheric conditions that are conducive for the development of midnight EPBs during the June solstice period. Hence, we employed SAMI2 model simulation to get the background electron density by inputting the $\boldsymbol{E}\times\boldsymbol{B}$ drift velocity obtained from the CINDI IVM onboard the C/NOFS satellite between 22:00–02:00 LT (Figure 4). The model simulation is carried out over EAR longitudinal sector (100.32° E) for the day number 172 (representing June Solstice) for the years 2010, 2011, 2012, and 2014 with the corresponding input parameters of solar activity and $\boldsymbol{E}\times\boldsymbol{B}$ drift values. Figure 5a–5d shows the vertical electron density distribution obtained from the SAMI2 model simulation during 22:00–02:00 LT (midnight period) over the magnetic equator for the years 2010, 2011, 2012, and 2014 respectively. The white curve in Figure 5a–5d indicates the mean $\boldsymbol{E}\times\boldsymbol{B}$ drift velocity values between 22:00–02:00 LT obtained from CINDI-IVM that fed to the SAMI2 model. It can be seen from Figure 5a–5d that the electron density is increasing with increasing solar activity from 2010 to 2014. Further, it can be observed that the F layer is elevated to higher altitudes during 2010 (~270 km around 01:00 LT) and gradually decreases with increasing solar activity in years 2011 (~260 km around 24:00 LT), 2012 (~250 km around 23:30 LT), and 2014 (~230 km around 24:00 LT).

In order to see the influence of vertical electron density distributions on the development of midnight EPBs, the flux tube integrated linear growth rate of RT instability is computed, similar to Ajith et al. (2016), by estimating the individual terms of the growth rate equation given by Sultan (1996), as

$$\gamma_{\mathrm{RT}} = \frac{\Sigma_P^F}{\Sigma_P^F + \Sigma_P^E}\left(V_P - U_L^P - \frac{g_e}{\nu_{\mathrm{eff}}^F}\right)K^F - R_T, \tag{1}$$

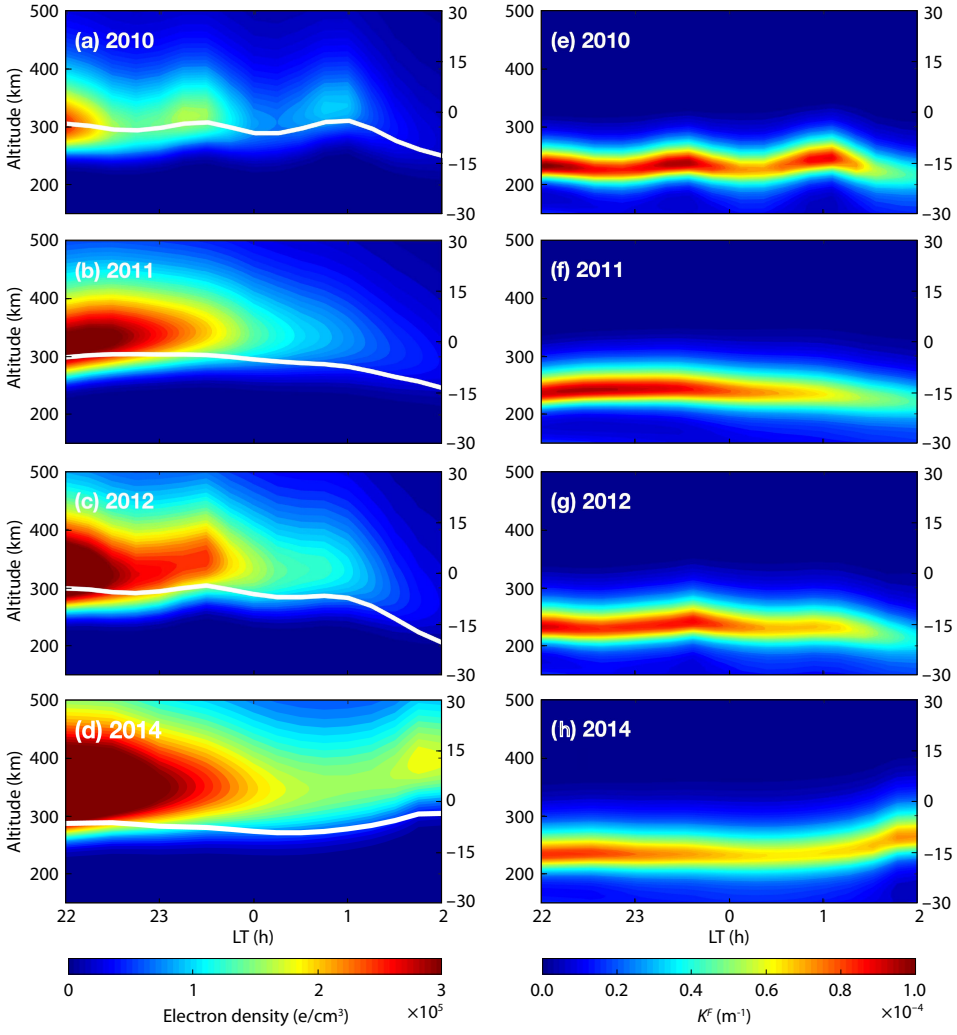

Figure 5. Altitude-local time variations of (a, b, c, and d) ionospheric electron density over magnetic equator derived from SAMI2 Model for day no. 172 (June solstice day), (f, g, h, and i) corresponding F region flux tube electron content height gradient (K^F) for the years 2010, 2011, 2012, and 2014 respectively.

where Σ_P^F and Σ_P^E are respectively the flux-tube integrated F region and E region Pedersen conductivities, V_P is the upward drift velocity, U_L^P is the flux tube integrated neutral wind perpendicular to the field line weighted by the Pedersen conductivity, g_e is the altitude corrected gravity, ν_{eff}^F is the flux tube integrated effective F region collision frequency weighted by the number density n_e, $K^F = \frac{1}{N_e}\left(\frac{\partial N_e}{\partial h}\right)$ is the vertical gradient of the field line integrated electron content in the F region, N_e is the flux tube electron content, and R_T is the flux tube integrated recombination rate. The detailed description of the flux tube integrated growth rate estimation can be seen in Ajith et al. (2016). Figure 5 (e–h) shows the altitudinal and local time variations of the F region flux tube electron content height gradient (K^F) for the years 2010, 2011, 2012, and 2014 respectively. It can be noticed from Figure 5e that, during the low solar activity year 2010 the steep density gradient region (high K^F) is at higher altitudes with maximum value of ~10 × 10^{-5} m^{-1} at an altitude of 240–280 km. The height and magnitude of the steep density gradient decreases slightly with increasing solar activity and reaches a minimum value of ~6.5 × 10^{-5} m^{-1} at an altitude of 200–250 km around 24:00 LT during the high solar activity year 2014.

Figure 6 (a–d) shows the flux tube integrated linear growth rate of RT instability (γ_{RT}) as a function of altitude and local time for the years 2010, 2011, 2012, and 2014 respectively. It can be observed from Figure 6a that, during the low solar activity year 2010, a significantly higher growth rate is observed between 22:00 to 02:00 LT, with a maximum value of ~6.5 × 10^{-4} s^{-1} around 24:00 LT. The

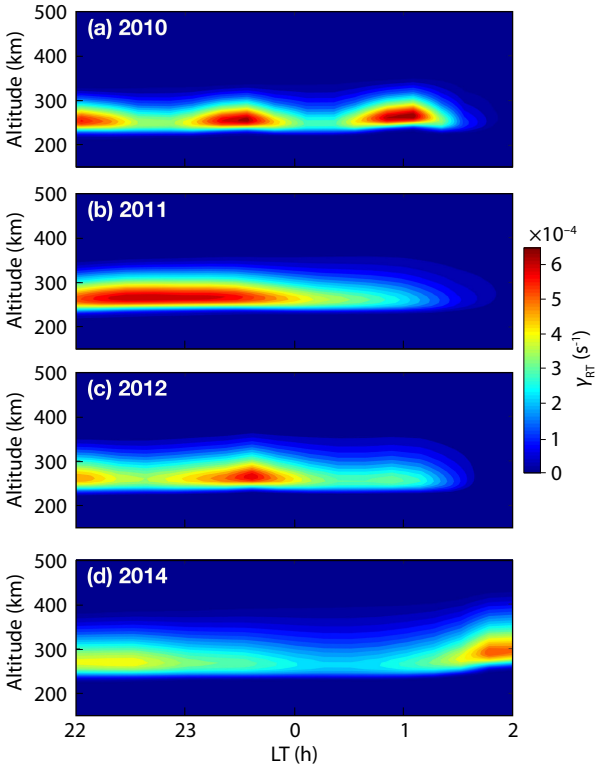

Figure 6. Altitude-local time variations of the flux tube integrated linear growth rate for RT instability (γ_{RT}) for the years (a) 2010, (b) 2011, (c) 2012, and (d) 2014 respectively.

presence of a steep density gradient region at higher altitude, where the ion neutral collision frequency (ν_{eff}^F) is negligible, results in the higher growth rate during this period. Further it can be noticed that the magnitude and local time extension of the growth rate decreases gradually with increasing solar activity. Finally, γ_{RT} is significantly reduced during the high solar activity year 2014, with a value of ~2 × 10^{-4} s^{-1} around the midnight hours. In a nutshell, the results presented in Figures 5 and 6 demonstrate the presence of a steep density gradient region at higher altitudes due to the elevated F layer, resulting in the higher RT instability growth rate during low solar activity years as compared to high solar activity years. This results in the enhanced development of fresh EPBs during the midnight hours of the low solar activity June solstice of 2010 (48.2%) as compared to the high solar activity year 2014 (5.4%).

4. Discussion

From Figure 2 it is clear that fresh occurrences of midnight EPBs are maximized during the low solar activity June solstice and decrease with increasing solar activity. This result is in good agreement with previous studies, which reported enhanced occurrence of midnight EPBs during the June solstice periods of low solar activity years (Otsuka et al., 2009; Yokoyama et al., 2011; Zhan WJ et al., 2018). Also, spatio-temporal observations based on the 2-dimensional fan-sector maps of EAR confirm without doubt that most of these EPBs observed over EAR longitudes evolve freshly during the midnight hours.

One of the most important factors responsible for the development of post-sunset EPBs is the elevation of the F layer by the strong eastward electric field due to the pre-reversal enhancement. Similarly, the results obtained in the present study show that, during the June soltice period of low solar activity years, the F layer is uplifted prior to the development of midnight EPBs. This result strongly corroborates previous observations (Niranjan et al., 2003; Nishioka et al., 2012; Ajith et al., 2015) and further confirms that the uplift of the F layer during summer time midnight hours is strongly dependent on solar activity. The uplifted F layer makes conditions favorable for the development of EPBs by the higher growth rate of RT instability due to the steep vertical density gradient at higher altitudes and the smaller ion-neutral collision frequency. These results confirm that the uplift of the F layer during low solar activity June solstice midnight hours is an important factor in the higher onset frequency of midnight EPBs.

The upward rise of the equatorial F region during these late-night hours is really puzzling and not yet fully understood. Several processes can contribute to upward drift of the F layer during low solar activity June solstices. The zonal electric field is generally westward during night time and can cause strong downward drift of the F region plasma at equatorial latitudes. However, the $\boldsymbol{E} \times \boldsymbol{B}$ drift observations from the IVM onboard the C/NOFS satellite in the present study (Figure 4) show that the downward drift due to the westward electric field is weak during the midnight hours of low solar activity years as compared to the high solar activity years. Similar observations of weakly downward $\boldsymbol{E} \times \boldsymbol{B}$ drift during the midnight hours of low solar activity June solstices were reported by Stoneback et al. (2011) and Ajith et al. (2016). Further, us-

ing drift mode ISR (Incoherent Scatter Radar) observations from Jicamarca, Zhan WJ and Rodrigues (2018) have shown that largely downward vertical drift velocity (~−20 m/s) has started to increase around 21:00 LT and becomes close to zero around the midnight hours of 4 June 2008. Hence, this weak westward electric field is one of the factors that keep the F layer at higher altitudes, due to the negligible downward drift of F region plasma during the midnight hours of low solar activity June solstices. There are several studies that report the effect of semi-diurnal tides as a probable reason for the enhanced zonal electric field during June soltice midnight hours (Stoneback et al., 2011; Sridharan and Meenakshi, 2020). From simultaneous observations using Ionosonde, MF radar, and C/NOFS over the Indian sector, Chakrabarty et al. (2014) showed that the mean amplitude of the meridional component of the semi diurnal tide during 2000–2011 increased with decreasing solar activity and was maximized during summer months of 2008. Further, they suggest that this semi-diurnal tide played a definite role in the enhancement of the zonal electric field during the June solstice of 2008, a low solar activity year.

Another factor favoring the upward drift of the F layer is the enhanced equatorward wind during the night time. The equatorward wind from both hemispheres can push the plasma along the field line, resulting in an uplift of the F layer over off-equatorial stations such as Kototabang. At equatorial latitudes, on the other hand, the direct effect of these equatorward meridional winds on the uplift of the F layer is insignificant due to the horizontal magnetic field lines over the equatorial region. However, the convergence of meridional neutral wind over the magnetic equator during the midnight hours (Maruyama et al., 2008; Ajith et al., 2016) can transport the plasma from off-equatorial regions along the field lines to higher altitudes over the equatorial region. According to Huba and Krall (2013) and Dao et al. (2017), the equatorward neutral wind can affect in two ways the uplifting of the F layer and the growth rate of RT instability. First, the component of the neutral wind along the magnetic field line (parallel component) can push the plasma to higher altitudes where the ion neutral collision frequency is smaller, reducing the Pedersen conductivity at the bottom side of the F region. Secondly, the component of the neutral wind transverse to the magnetic field (perpendicular component) can result in an eastward Pedersen current. Later, using SAMI2 model simulations, Zhan WJ and Rodrigues (2018) showed that the converging neutral wind, in the presence of a weak westward electric field, increases the destabilizing effect of the F region plasma in the midnight period. So far, several studies (for example. Niranjan et al., 2003; Maruyama et al., 2008; Dao et al., 2017) have sought possible mechanisms for the enhanced equatorward wind and its convergence over the magnetic equator during low solar activity June soltice midnight hours; these studies have reported that the Midnight Temperature Maximum (MTM) has a major role in the enhanced equatorward meridional wind. Using model simulations (Fesen, 1996) and observations (Niranjan et al., 2003), it was confirmed that the MTM occurs earlier and much more strongly in the low solar activity summer months. Further, using numerical simulations, Fang TW et al. (2016) showed that the local dynamics associated with MTM at thermospheric altitudes plays an important role in the upward drift in the night-time equatorial ionosphere. Further, during June solstices, the transequatorial neutral wind blows from the north hemisphere (summer) to the south hemisphere (winter) due to northward migration of the sub-solar point (Maruyama et al., 2007). This summer to winter transequatorial wind results in larger upward transports of plasma in the northern hemisphere and can contribute to the larger increase in the *h*′F over Chumphon during the June solstice midnight hours, as shown in Figure 3.

Finally, the flux tube integrated linear growth rates of RT instability estimated for the years 2010, 2011, 2012, and 2014 show a maximized growth rate during the low solar activity year 2010. The gradual decrease of growth rate with increasing solar activity and the significant reduction in the growth rate during the high solar activity year 2014 are also clear from Figure 6. The presence of a weak westward electric field and enhanced equatorward neutral wind during the midnight hours of low solar activity June solstice sets the favorable conditions for the development of EPBs by keeping the F layer at higher altitudes with higher RT instability growth rates. This result is in good agreement with previous studies (Nicolls et al., 2006; Ajith et al., 2016; Zhan WJ and Rodrigues., 2018).

In addition to the aforementioned factors, how the threshold height required for the development of EPBs varies with solar activity needs to be discussed. From previous studies it is clear that the threshold height required for EPB onset decreases with declining solar activity (Jayachandran et al., 1993; Jyoti et al., 2004; Tulasi Ram et al., 2007). Tulasi Ram et al. (2007) studied the solar activity dependence of the threshold height required for the development of EPBs by estimating the local linear growth rate of RT instability. They found that the threshold base height of the F-layer for the development of EPBs at 19:00 LT over the equator fell from 405 km to 317 km as the solar activity decreased from March 2001 to March 2005. Recently, Ajith et al. (2016) have shown that a given growth rate of RT instability (γ_{RT}) can be achieved at a lower altitude during June solstice midnight hours, compared to the equinoctial post-sunset period. Further, observations from EAR show that the initial altitude of EPB onset is significantly lower during post-midnight periods compared to post-sunset hours (Ajith et al., 2015; Dao T et al., 2016). Therefore, even a smaller height rise during the midnight hours of the solar minimum period can initiate RT instability and the further development of EPBs.

The seeding of RT instability by medium-scale traveling ionospheric disturbances (MSTIDs) is another possible factor in the development of midnight EPBs during low solar activity June solstices (Miller et al., 2009; Yokoyama et al., 2011). The MSTIDs at ionospheric altitudes can modulate the bottom side of the ionosphere, and their quasi-sinusoidal nature can provide the required seed perturbation for RT instability (Taori et al., 2015). From simultaneous observations using an airglow imager and VHF radar, Miller et al. (2009) showed the development of midnight EPBs just after the presence of southwestward propagating MSTIDs. The occurrence of night-time MSTIDs is maximized during the summer and often propagates in the southwestward direction (Otsuka et al., 2011; Ding et al., 2011). Generally, the equatorward propagation of MSTIDs is inhibited by the increased ion drag due to the equatorial ionization anomaly (EIA) crest (Shiokawa et al.,

2002). However, it has been observed that the MSTIDs could pass through the EIA crest and reach very close to the magnetic equator during solar minimum years (Makela et al., 2010; Narayanan et al., 2014). Therefore, these low latitude MSTIDs could act as seeding sources for RT instability, and thus trigger conditions more favorable to the development of EPBs during low solar activity June solstices.

5. Summary

Data from the 47 MHz Equatorial Atmosphere Radar at Kototabang, Indonesia were used to investigate the influence of solar activity on the occurrence of the summertime midnight EPBs during the ascending phase of solar cycle 24, from 2010–2014. FAI observations from EAR show that the occurrence was at its maximum during the low solar activity year 2010 and decreased monotonically thereafter with increasing solar activity. The bottom-side F layer virtual height observations from Chumphon and Kototabang ionosondes show the elevated F layer during the midnight hours of low solar activity June solstices. Using realistic E x B drift velocity data obtained from the CINDI-IVM onboard the C/NOFS satellite, the physics-based SAMI2 model has been employed to simulate the background ionospheric electron density, and the fluxtube integrated RT instability growth rate has been estimated. The results show that higher growth rates are observed during the midnight hours of low solar June solstices, which corresponds to the high EPB occurrence observed by EAR during those periods. The relatively higher F layer and the formation of the steep density gradient (high K^F) region at higher altitude are the key factors favoring the enhanced growth rate of RT instability during the midnight hours of low solar activity years. The factors responsible for conditions favorable to the generation of summer time midnight EPBs are discussed in light of the elevated F layer due to the weak westward electric field in the presence of equatorward neutral wind and the possible seeding of RT instability by MSTIDs.

Acknowledgments

This work was partly supported by the National Natural Science Foundation of China (42020104002) and by a Postdoctoral Fellowship at the Institute of Geology and Geophysics, Chinese Academy of Sciences (IGGCAS). K. Hozumi was partially supported by JSPS KAKENHI Grant Number 20H00197. The EAR data can be obtained from http://www.rish.kyoto-u.ac.jp/ear/index-e.html. The CPN and KTB ionosonde data are available under SEALION network at https://aer-nc-web.nict.go.jp/sealion/. The CINDI-IVM data are provided through the auspices of the CINDI team at the University of Texas at Dallas, supported by NASA grant NAS5-01068 (https://cdaweb.gsfc.nasa.gov/index.html/). The $F_{10.7}$ cm solar flux is obtained from https://omniweb.gsfc.nasa.gov/form/dx1.html.

References

Aarons, J., Mullen, J. P., Whitney, H. E., and Mackenzie, E. M. (1980). The dynamics of equatorial irregularity patch formation, motion, and decay. *J. Geophys. Res.*, *85*(A1), 139–149. https://doi.org/10.1029/JA085iA01p00139

Ajith, K. K., Tulasi Ram, S., Yamamoto, M., Yokoyama, T., Gowtam, V. S., Otsuka, Y., Tsugawa, T., and Niranjan, K. (2015). Explicit characteristics of evolutionary-type plasma bubbles observed from Equatorial Atmosphere Radar during the low to moderate solar activity years 2010-2012. *J. Geophys. Res.*, *120*(2), 1371–1382. https://doi.org/10.1002/2014JA020878

Ajith, K. K., Tulasi Ram, S., Yamamoto, M., Otsuka, Y., and Niranjan, K. (2016). On the fresh development of equatorial plasma bubbles around the midnight hours of June solstice. *J. Geophys. Res.*, *121*(9), 9051–9062. https://doi.org/10.1002/2016JA023024

Chakrabarty, D., Fejer, B. G., Gurubaran, S., Pant, T. K., Abdu, M. A., and Sekar, R. (2014). On the pre-midnight ascent of F-layer in the June solstice during the deep solar minimum in 2008 over the Indian sector. *J. Atmos. Terr. Phys.*, *121*, 177–187. https://doi.org/10.1016/j.jastp.2014.01.002

Dao, T., Otsuka, Y., Shiokawa, K., Tulasi Ram, S., and Yamamoto, M. (2016). Altitude development of postmidnight *F* region field-aligned irregularities observed using Equatorial Atmosphere Radar in Indonesia. *Geophys. Res. Lett.*, *43*(3), 1015–1022. https://doi.org/10.1002/2015GL067432

Dao, T., Otsuka, Y., Shiokawa, K., Nishioka, M., Yamamoto, M., Buhari, S. M., Abdullah, M., and Husin, A. (2017). Coordinated observations of postmidnight irregularities and thermospheric neutral winds and temperatures at low latitudes. *J. Geophys. Res.*, *122*(7), 7504–7518. https://doi.org/10.1002/2017JA024048

de La Beaujardière, O., and The C/NOFS Science Definition Team. (2004). C/NOFS: a mission to forecast scintillations. *J. Atmos. Sol. Terr. Phys.*, *66*(17), 1573–1591. https://doi.org/10.1016/j.jastp.2004.07.030

Ding, F., Wan, W. X., Xu, G. R., Yu, T., Yang, G. L., and Wang, J. S. (2011). Climatology of medium-scale traveling ionospheric disturbances observed by a GPS network in central China. *J. Geophys. Res.*, *116*(A9), A09327. https://doi.org/10.1029/2011JA016545

Fang, T. W., Akmaev, R. A., Stoneback, R. A., Fuller-Rowell, T., Wang, H., and Wu, F. (2016). Impact of midnight thermosphere dynamics on the equatorial ionospheric vertical drifts. *J. Geophys. Res.*, *121*(5), 4858–4868. https://doi.org/10.1002/2015JA022282

Fejer, B. G., Farley, D. T., Woodman, R. F., and Calderon, C. (1979). Dependence of Equatorial *F* region vertical drifts on season and solar cycle. *J. Geophys. Res.*, *84*(A10), 5792–5796. https://doi.org/10.1029/JA084iA10p05792

Fesen, C. G. (1996). Simulations of the low-latitude midnight temperature maximum. *J. Geophys. Res.*, *101*(A12), 26863–26874. https://doi.org/10.1029/96JA01823

Fukao, S., Hashiguchi, H., Yamamoto, M., Tsuda, T., Nakamura, T., Yamamoto, M. K., Sato, T., Hagio, M., and Yabugaki, Y. (2003). Equatorial Atmosphere Radar (EAR): system description and first results. *Radio Sci.*, *38*(3), 1053. https://doi.org/10.1029/2002RS002767

Haerendel, G. (1973). Theory of equatorial spread F, preprint, Max-Planck-Institut fur Physik and Astrophysik, Institut fur Extraterrestrisches Physik, Garching, West Germany.

Heelis, R. A., Stoneback, R., Earle, G. D., Haaser, R. A., and Abdu, M. A. (2010). Medium-scale equatorial plasma irregularities observed by Coupled Ion-Neutral Dynamics Investigation sensors aboard the Communication Navigation Outage Forecast System in a prolonged solar minimum. *J. Geophys. Res.*, *115*(A10), A10321. https://doi.org/10.1029/2010JA015596

Huba, J. D., Joyce, G., and Fedder, J. A. (2000). Sami2 is AnotherModel of the Ionosphere (SAMI2): a new low-latitude ionosphere model. *J. Geophys. Res.*, *105*(A10), 23035–23053. https://doi.org/10.1029/2000JA000035

Huba, J. D., and Krall, J. (2013). Impact of meridional winds on equatorial spread *F*: revisited. *Geophys. Res. Lett.*, *40*(7), 1268–1272. https://doi.org/10.1002/grl.50292

Jayachandran, B., Balan, N., Rao, P. B., Sastri, J. H., and Bailey, G. J. (1993). HF Doppler and ionosonde observations on the onset conditions of equatorial spread F. *J. Geophys. Res.*, *98*(A8), 13741–13750. https://doi.org/10.1029/93JA00302

Jyoti, N., Devasia, C. V., Sridharan, R., and Tiwari, D. (2004). Threshold height $(h'F)_c$ for the meridional wind to play a deterministic role in the bottom side equatorial spread F and its dependence on solar activity. *Geophys. Res. Lett.*, *31*(12), L12809. https://doi.org/10.1029/2004GL019455

Krishna Moorthy, K., Raghava Reddi, C., and Krishna Murthy, B. V. (1979). Night time ionospheric scintillations at the magnetic equator. *J. Atmos. Terr. Phys.*, *41*(2), 123–134. https://doi.org/10.1016/0021-9169(79)90004-7

Li, G. Z., Ning, B. Q., Abdu, M. A., Yue, X. A., Liu, L. B., Wan, W. X., and Hu, L. H.

(2011). On the occurrence of postmidnight equatorial *F* region irregularities during the June solstice. *J. Geophys. Res.*, *116*(A4), A04318. https://doi.org/10.1029/2010JA016056

Makela, J. J., Miller, E. S., and Talaat, E. R. (2010). Nighttime medium-scale traveling ionospheric disturbances at low geomagnetic latitudes. *Geophys. Res. Lett.*, *37*(24), L24104. https://doi.org/10.1029/2010GL045922

Maruyama, T., Kawamura, M., Saito, S., Nozaki, K., Kato, H., Hemmakorn, N., Boonchuk, T., Komolmis, T., and Ha Duyen C. (2007). Low latitude ionosphere-thermosphere dynamics studies with inosonde chain in Southeast Asia. *Ann. Geophys.*, *25*(7), 1569–1577. https://doi.org/10.5194/angeo-25-1569-2007

Maruyama, T., Saito, S., Kawamura, M., and Nozaki, K. (2008). Thermospheric meridional winds as deduced from ionosonde chain at low and equatorial latitudes and their connection with midnight temperature maximum. *J. Geophys. Res.*, *113*(A9), A09316. https://doi.org/10.1029/2008JA013031

Miller, E. S., Makela, J. J., and Kelley, M. C. (2009). Seeding of equatorial plasma depletions by polarization electric fields from middle latitudes: experimental evidence. *Geophys. Res. Lett.*, *36*(18), L18105. https://doi.org/10.1029/2009GL039695

Narayanan, V. L., Shiokawa, K., Otsuka, Y., and Saito, S. (2014). Airglow observations of nighttime medium-scale traveling ionospheric disturbances from Yonaguni: Statistical characteristics and low-latitude limit. *J. Geophys. Res.*, *119*(11), 9268–9282. https://doi.org/10.1002/2014JA020368

Nicolls, M. J., Kelley, M. C., Vlasov, M. N., Sahai, Y., Chau, J. L., Hysell, D. L., Fagundes, P. R., Becker-Guedes, F., and Lima, W. L. C. (2006). Observations and modeling of post-midnight uplifts near the magnetic equator. *Ann. Geophys.*, *24*(5), 1317–1331. https://doi.org/10.5194/angeo-24-1317-2006

Niranjan, K., Brahmanandam, P. S., Ramakrishna Rao, P., Uma, G., Prasad, D. S. V. V. D., and Rama Rao, P. V. S. (2003). Post-midnight spread-F occurrence over Waltair (17.7° N, 83.3° E) during low and ascending phases of solar activity. *Ann. Geophys.*, *21*(3), 745–750. https://doi.org/10.5194/ANGEO-21-745-2003

Nishioka, M., Otsuka, Y., Shiokawa, K., Tsugawa, T., Effendy, Supnithi, P., Nagatsuma, T., and Murata, K. T. (2012). On post-midnight field-aligned irregularities observed with a 30.8-MHz radar at a low latitude: comparison with *F*-layer altitude near the geomagnetic equator. *J. Geophys. Res.*, *117*(A8), A08337. https://doi.org/10.1029/2012JA017692

Otsuka, Y., Ogawa, T., and Effendy. (2009). VHF radar observations of night time F-region field-aligned irregularities over Kototabang, Indonesia. *Earth, Planets Space*, *61*(4), 431–437. https://doi.org/10.1186/BF03353159

Otsuka, Y., Kotake, N., Shiokawa, K., Ogawa, T., Tsugawa, T., and Saito, A. (2011). Statistical study of medium-scale traveling ionospheric disturbances observed with a GPS receiver network in Japan. In M. A. Abdu, et al. (Eds.), *Aeronomy of the Earth's Atmosphere and Ionosphere* (pp. 291-299). Dordrecht, Netherlands: Springer.

Patra, A. K., Phanikumar, D. V., and Pant, T. K. (2009). Gadanki radar observations of *F* region field-aligned irregularities during June solstice of solar minimum: first results and preliminary analysis. *J. Geophys. Res.*, *114*(A12), A12305. https://doi.org/10.1029/2009JA014437

Shiokawa, K., Otsuka, Y., Ejiri, M. K., Sahai, Y., Kadota, T., Ihara, C., Ogawa, T., Igarashi, K., Miyazaki, S., and Saito, A. (2002). Imaging observations of the equatorward limit of midlatitude traveling ionospheric disturbances. *Earth, Planets Space*, *54*(1), 57–62. https://doi.org/10.1186/BF03352421

Sridharan, S., and Meenakshi, S. (2020). Semidiurnal tidal influence on the occurrence of postmidnight *F* region FAI radar echoes. *J. Geophys. Res.*, *125*(8), e2019JA027700. https://doi.org/10.1029/2019JA027700

Stoneback, R. A., Heelis, R. A., Burrell, A. G., Coley, W. R., Fejer, B. G., and Pacheco, E. (2011). Observations of quiet time vertical ion drift in the equatorial ionosphere during the solar minimum period of 2009. *J. Geophys. Res.*, *116*(A12), A12327. https://doi.org/10.1029/2011JA016712

Subbarao, K. S. V., and Krishna Murthy, B. V. (1994). Post-sunset *F*-region vertical velocity variations at magnetic equator. *J. Atoms. Terr. Phys.*, *56*(1), 59–65. https://doi.org/10.1016/0021-9169(94)90176-7

Sultan, P. J. (1996). Linear theory and modeling of the Rayleigh-Taylor instability leading to the occurrence of equatorial spread F. *J. Geophys. Res.*, *101*(A12), 26875–26891. https://doi.org/10.1029/96JA00682

Taori, A., Parihar, N., Ghodpage, R., Dashora, N., Sripathi, S., Kherani, E. A., and Patil, P. T. (2015). Probing the possible trigger mechanisms of an equatorial plasma bubble event based on multistation optical data. *J. Geophys. Res.*, *120*(10), 8835–8847. https://doi.org/10.1002/2015JA021541

Tulasi Ram, S., Rama Rao, P. V. S., Niranjan, K., Prasad, D. S. V. V. D., Sridharan, R., Devasia, C. V., and Ravindran, S. (2006). The role of post-sunset vertical drifts at the equator in predicting the onset of VHF scintillations during high and low sunspot activity years. *Ann. Geophys.*, *24*(6), 1609–1616. https://doi.org/10.5194/angeo-24-1609-2006

Tulasi Ram, S., Rama Rao, P. V. S., Prasad, D. S. V. V. D., Niranjan, K., Raja Babu, A., Sridharan, R., Devasia, C. V., and Ravindran, S. (2007). The combined effects of electrojet strength and the geomagnetic activity (K_p-index) on the post sunset height rise of the *F*-layer and its role in the generation of ESF during high and low solar activity periods. *Ann. Geophys.*, *25*(9), 2007–2017. https://doi.org/10.5194/angeo-25-2007-2007,2007

Tulasi Ram, S., Ajith, K. K., Yokoyama, T., Yamamoto, M., and Niranjan, K. (2017). Vertical rise velocity of equatorial plasma bubbles estimated from Equatorial Atmosphere Radar (EAR) observations and HIRB model simulations. *J. Geophys. Res.*, *122*(6), 6584–6594. https://doi.org/10.1002/2017JA024260

Yizengaw, E., Retterer, J., Pacheco, E. E., Roddy, P., Groves, K., Caton, R., and Baki, P. (2013). Postmidnight bubbles and scintillations in the quiet-time June solstice. *Geophys. Res. Lett.*, *40*(21), 5592–5597. https://doi.org/10.1002/2013GL058307

Yokoyama, T., Fukao, S., and Yamamoto, M. (2004). Relationship of the onset of equatorial *F* region irregularities with the sunset terminator observed with the Equatorial Atmosphere Radar. *Geophys. Res. Lett.*, *31*(24), L24804. https://doi.org/10.1029/2004GL021529

Yokoyama, T., Yamamoto, M., Otsuka, Y., Nishioka, M., Tsugawa, T., Watanabe, S., and Pfaff, R. F. (2011). On postmidnight low-latitude ionospheric irregularities during solar minimum: 1. Equatorial Atmosphere Radar and GPS-TEC observations in Indonesia. *J. Geophys. Res.*, *116*(A11), A11325. https://doi.org/10.1029/2011JA016797

Zhan, W. J., and Rodrigues, F. S. (2018). June solstice equatorial spread *F* in the American sector: a numerical assessment of linear stability aided by incoherent scatter radar measurements. *J. Geophys. Res.*, *123*(1), 755–767. https://doi.org/10.1002/2017JA024969

Zhan, W. J., Rodrigues, F. S., and Milla, M. A. (2018). On the genesis of postmidnight equatorial spread *F*: results for the American/Peruvian sector. *Geophys. Res. Lett.*, *45*(15), 7354–7361. https://doi.org/10.1029/2018GL078822